

Article

Local Climate Zones, Land Surface Temperature and Air Temperature Interactions: Case Study of Hradec Králové, the Czech Republic

Hana Středová ^{1,2}, Filip Chuchma ² , Jaroslav Rožnovský ^{1,2} and Tomáš Středa ^{1,2,*} 

¹ Mendel University in Brno, 613 00 Brno, Czech Republic; hana.stredova@mendelu.cz (H.S.); jaroslav.roznovsky@mendelu.cz (J.R.)

² Czech Hydrometeorological Institute, Branch Office Brno, 616 67 Brno, Czech Republic; filip.chuchma@chmi.cz

* Correspondence: streda@mendelu.cz

Abstract: The current application of local climate zones (LCZs) often ends with (inter)zonal comparison of land surface temperature (LST) or air temperature (AT). LST evaluation employs an enhanced concept of LCZs together with cluster analysis for LCZs grouped based on LST. The paper attempts to combine them into a complex approach derived from the case study on a medium-sized Central European city (Hradec Králové, the Czech Republic). In particular, the paper addresses the following. (i) The relation of LST and AT, when the daily course of temperature profile ranging clear off the surface up to 2 m was fitted by a rational 2D function. The obtained equation enables derivation of the AT from LST and vice versa. (ii) The differences in thermal response of LCZs based on LST or AT, where the highest average LST and average maximum LST show LCZs 10, 2, 3 and 8, i.e., with a significant proportion of artificial surfaces. The cluster of LCZs with a significant representation of vegetation, LCZs 9, B, D, A and G, have significantly lower LST. (iii) The contribution of LCZs to understanding of LST/AT relation and whether their specific relation could be expected in particular LCZs, when subsequent interaction assessment of LST and AT revealed statistically their significant correlation in LCZs for certain cases.

Keywords: urban environment; urban climate; urban heat island; cluster analysis; artificial surfaces; human health; environmental health



Citation: Středová, H.; Chuchma, F.; Rožnovský, J.; Středa, T. Local Climate Zones, Land Surface Temperature and Air Temperature Interactions: Case Study of Hradec Králové, the Czech Republic. *ISPRS Int. J. Geo-Inf.* **2021**, *10*, 704. <https://doi.org/10.3390/ijgi10100704>

Academic Editor: Wolfgang Kainz

Received: 29 August 2021

Accepted: 12 October 2021

Published: 15 October 2021

Publisher's Note: MDPI stays neutral with regard to jurisdictional claims in published maps and institutional affiliations.



Copyright: © 2021 by the authors. Licensee MDPI, Basel, Switzerland. This article is an open access article distributed under the terms and conditions of the Creative Commons Attribution (CC BY) license (<https://creativecommons.org/licenses/by/4.0/>).

1. Introduction

Increasing urbanization and related issues such as the formation of specific urban environments deserves enormous attention of all the relevant stakeholders including scientists, as 70% of the global population is predicted to live in cities by 2050 [1]. Radiation affected by urban geometry, effect of artificial materials on heat accumulation and radiation [2] and redundant heat conducted from buildings [3] are the main factors causing urban heat island (UHI). UHI effect is strengthened mainly during summer and autumn warm, windless and cloudless days [4]. The very first survey that compared the course of temperature in urban areas with surrounding landscape was the Climate of London analysis published by [5]. High air temperature (AT) in urban areas and especially their long-term occurrence in so-called heat waves cause intensive physical stress with negative impacts on human health. It was found that summer mortality in big cities was strongly associated with hot weather and heat wave duration and severity as reported by [6] for Shanghai, [7] for Chicago, [8] for Lisbon, [9] for Paris, [10] for Montreal and [11] from a city located in temperate climate. However, though the severity of heat waves did not increase generally during the 20th century, their incidence is predicted to alter dramatically, especially in the second half of the 21st century [12]. A negative impact of UHI on human health might be further strengthened by various attendant effects such as noise and light pollution [13–15]

and various sources of chemical pollutants. More than 100 indices have been developed and used to assess bioclimatic conditions for humans. Among the most frequently used is HUMIDEX (humidity index), UTCI (Universal Thermal Climate Index), and HI (Heat Index). Comparison of several thermal indices and their pros and cons analysis was carried out in [16].

Urban areas with a unique temperature regime (parking lots, industrial objects, flat roofs, asphalt roads, etc.) producing “hot spots” within a city, are occasionally referred to as a “micro-urban heat island” MUHI [17–19] or in terms of land surface temperature (LST) as “surface urban heat island” (SUHI) [20]. According to study of [21] the highest SUHI occurred in densely built-up and industrial zones, and the lowest in sparsely built city outskirts.

Knowledge of local geographical conditions and the surface temperature regime enable identification of places with thermal and/or thermodynamically related local climatic effects [22]. A study of [23] identifies 17 types of urban terrain zones (UTZ) to classify the physical structure of cities. The method of urban morphometry based on aerial photography is globally applicable. Another classification of distinct urban forms according to their ability to influence local climate breaks city terrain down into seven homogenous regions called “urban climate zones” (UCZ) [24].

The schemes on the urban morphology standardization are a concept of local climate zones (LCZ) suggested by [25], which is based on the same principles as the former simplified classification of urban climate zones (UCZ) by [24]. The classification of LCZs represents an up-to-date concept for the classification and unification of the sites with analogous effect on climate. Studies [26,27] created the first LCZs mapping methods and enhanced the LCZ concept towards a generally recognized regional typology.

The LCZ classification has found wide acceptance and application in a range of urban climate investigations. The review study [28] revealed that LCZ classification has proven to be a universally applicable method of description of the physical environment for the purposes of urban climate research. Researchers, however, frequently doubt which LCZ should be assigned, and how to indicate sub-classes. Mapping of LCZs is itself complicated, because similar LCZs in different regions have dissimilar spectral properties due to differences in vegetation, building materials and other variations with respect to local and physical environmental factors. Research and development is the appropriate universal protocol of LCZs mapping, with easy-to-understand workflow which uses freely available data and software and is applicable by someone without specialist knowledge in spatial analysis or urban climate science [29].

A number of authors dealing with LCZs have pointed out that the influence of thermal and radiative attributes and surface properties on the local climate may significantly vary with the broader geographical location of the city, actual location of LCZ within the city and with city size and its relief [30,31]. Geletič and Lehnert (2016) [32] designed a new GIS-based LCZ mapping method for Central European cities and compiled LCZ maps for medium-sized Central European cities (modification of [24] concept of LCZs). The method is based on measurable physical properties and a precisely defined decision-making algorithm. Even though there are various studies on UHI based on LCZs, they generally deal either with LST (e.g., [33]) or with AT (e.g., [34]).

The current real application of LCZ concept often ends with the description of (inter) zonal comparison of LST or AT. A comprehensive method combining LCZs, LST and AT is still rare (e.g., [35]). For this reason, we are offering the case study combining LCZ, LST and AT into a complex approach. Although the model based on this case study is, of course, not universally valid, it is contributory from a methodological point of view. In particular, the paper addresses: (i) the relation of LST and AT and points out why it is important to study it; (ii) the differences in thermal response of LCZs if it is based on surface or AT; (iii) LCZs' contribution to understanding of surface–air temperature relation/interaction and whether a specific relation of surface–air temperature in particular LCZs could be expected. Along with that, we point out general obstacles and limits of LCZ application which might lead to

misinterpretations or misleading conclusions. In order to do so, we employ three particular but consequent case studies carried out for a Central European medium-sized city.

2. Materials and Methods

Complex methodological approach is summarized in five-step flowchart (Figure 1) and subsequently described in detail in Sections 2.1–2.5.

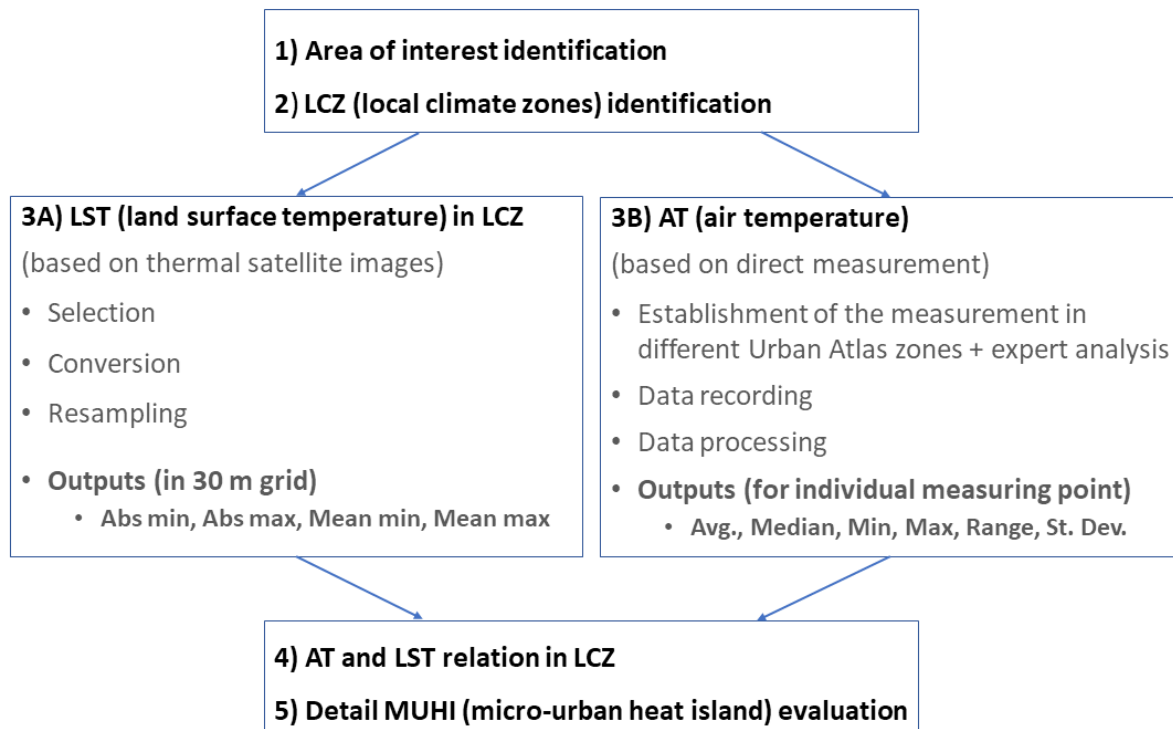


Figure 1. The methodological flowchart.

2.1. Area of Interest

Hradec Králové with a population of nearly one-hundred thousand and an area of 105.6 km² is one of the ten biggest cities in the Czech Republic (Central Europe), see Figure 2. The landscape is predominantly flat with an average altitude of 235 MASL. The mean annual temperature (1961–1990) is 8.7 °C, and the mean annual precipitation total is 600.2 mm. The warmest months are July (18.3 °C) and August (17.8 °C). Future climatic trend using a regional climatic model ALADIN-Climate/CZ and A1B emission scenario (according to the IPCC) predicts an increase in mean annual temperature up to 9.9 °C in 2021–2050 and August to be the warmest month with a mean temperature of 21.0 °C [36]. According to Köppen climate classification [37], the area falls within climatic region Cfb (temperate oceanic climate). The immediate surrounding area is mostly arable land and suburban forests (Figure 3). Based on data of the Czech statistical office the area of green vegetation per inhabitant is one of the highest among the large Czech cities. In addition, the confluence of the Labe and Orlice Rivers in the city center significantly influences surrounding climate. The initiatives on UHI investigation in this city came from local authorities in broader context of urban planning respecting the scientific findings on local climate.

2.2. Local Climate Zones Identification

A GIS-based approach [32] was used for LCZs delimitation to make our study comparable with studies on other cities (Figure 4 and Table 1). The algorithm of the LCZs delimitation derives from the basic physical parameters defined by [25]: building surface fraction, pervious surface fraction, impervious surface fraction and height of roughness

elements. For further sub-classification of 100×100 cells belonging to LCZ land cover types (A–G), the algorithm uses information from the ZABAGED geodatabase. Thus, each cell (100×100) is allocated to an appropriate LCZ. At the end of the classification process, a two-stage majority filter was applied to define LCZs. When all cells had been assigned to an appropriate LCZ, the LCZ areas were delineated using a majority filter to smooth the results of classification. Independent testing of the decision-making algorithm for defining the percentage coverage for individual LCZs demonstrated close agreement with areas defined on the basis of expert knowledge. Therefore, the final results of classification were validated using expert knowledge [32,33].

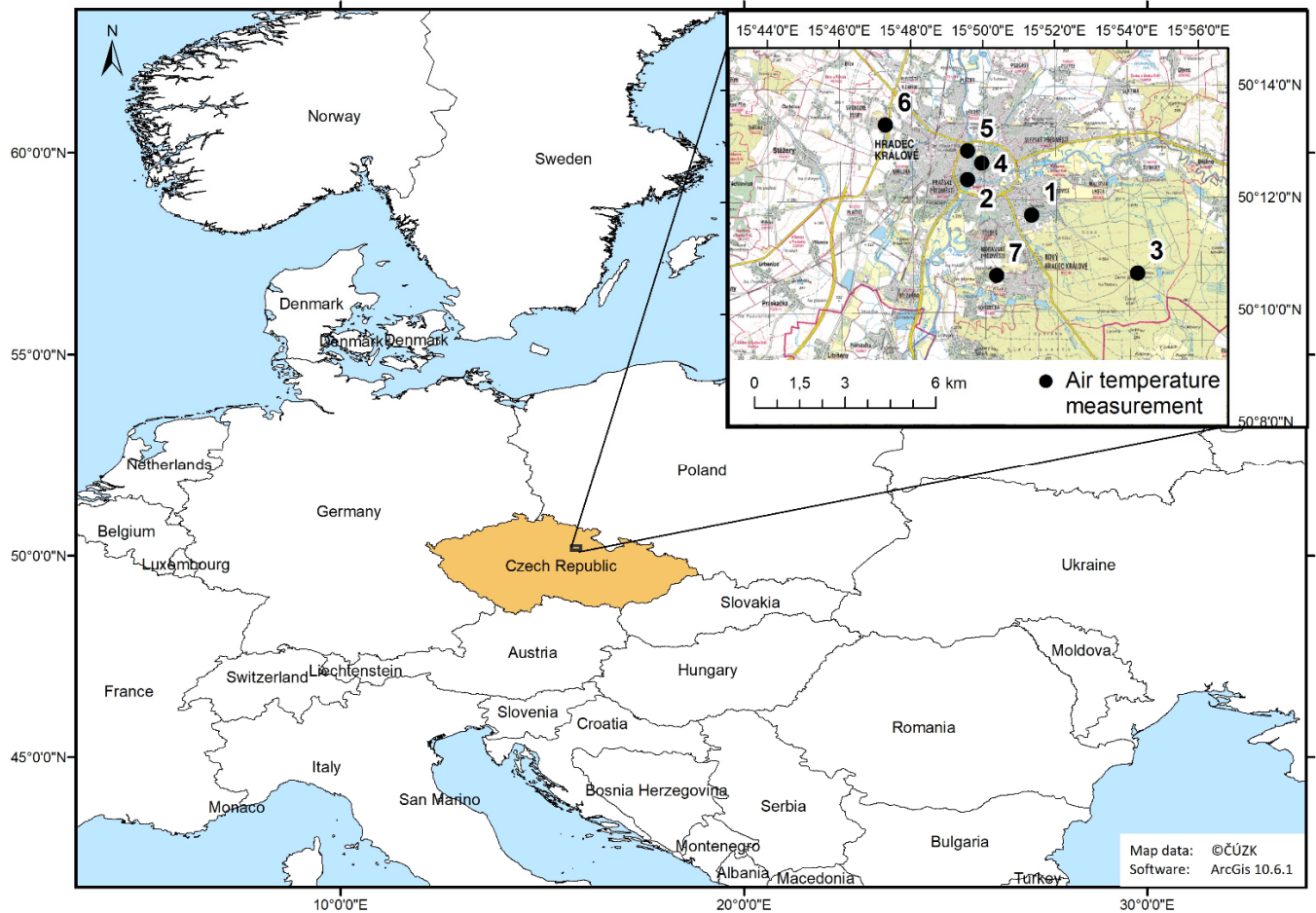


Figure 2. Location of the study area. Map data: © Czech Office for Surveying, Mapping and Cadastre (ČÚZK).

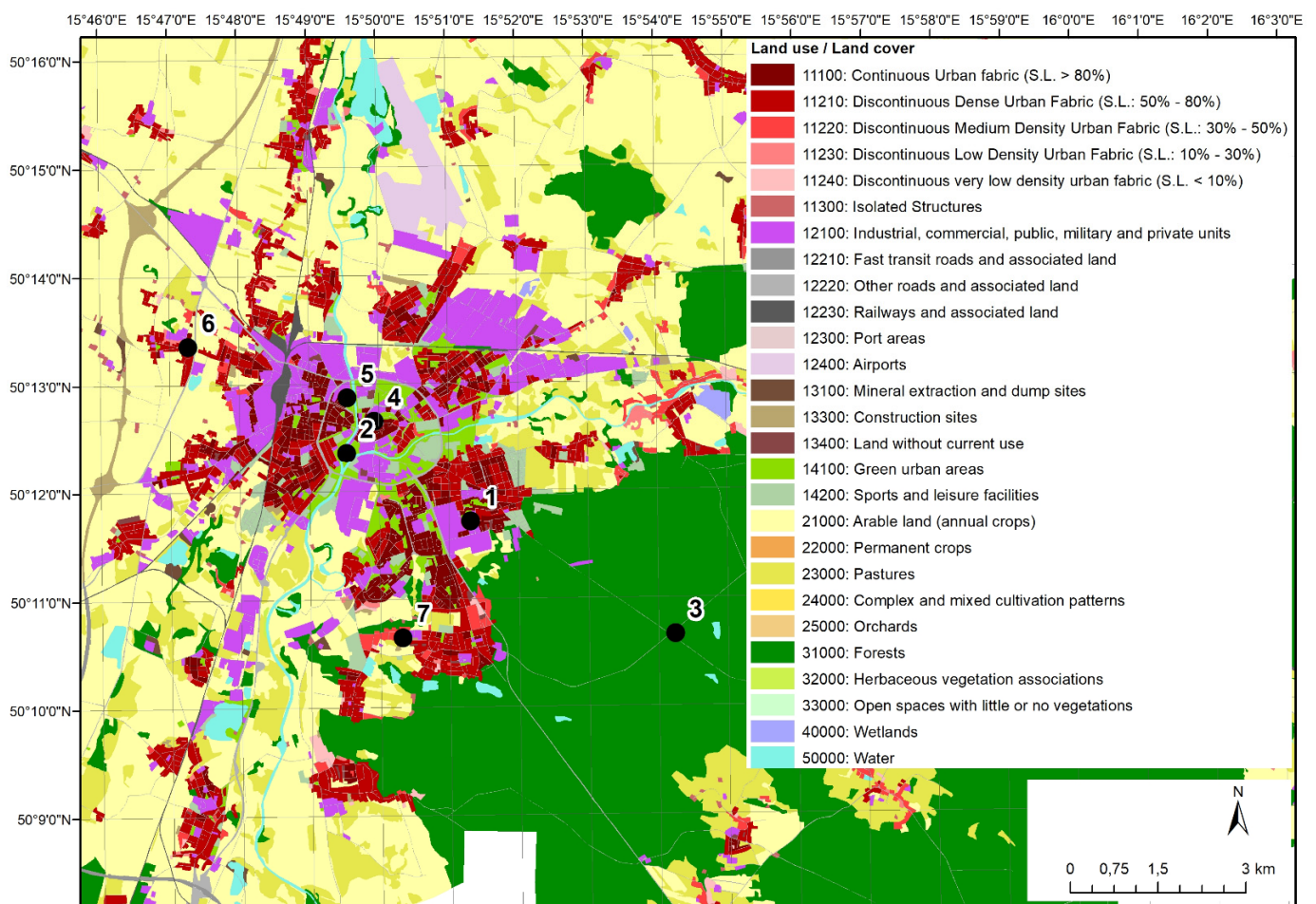


Figure 3. The land use/land cover of study area with marked AT measurement network–Section 2.3B (points numbered 1–7). Data from [38].

2.3. LST and AT Evaluation

(A) LST evaluation:

LST was derived from LANDSAT-8 satellite through the U.S. Geological Survey [39] with the thermal infrared sensors (TIRS) with two bands (10 and 11), collected at 100-m resolution (for the infrared thermal bands) and resampled to 30 m.

Identification of proper scenes: Images from the LANDSAT-8 (TIRS sensor) satellite were used for LST analysis, analysis of LST differences in individual LCZs and evaluation of the link between LST and AT from ground monitoring. The scenes under investigation have to meet following requirements: (i) the date thermal images corresponds to AT monitoring term (see “Ad hoc monitoring of AT”); (ii) represent days with a high AT (tropical days) and a high value of global radiation when the highest impact of artificial surfaces on AT is expected; (iii) represent days which followed a day with a maximum AT of at least 30 °C for reference climatological location; (iv) frame time of the day with a demonstrable effect of global radiation on LST; (v) scene cloud cover less than 2 percent. Based on this selection procedure two scenes were selected for detailed analysis. Basic scene information is summarized in Table 2.

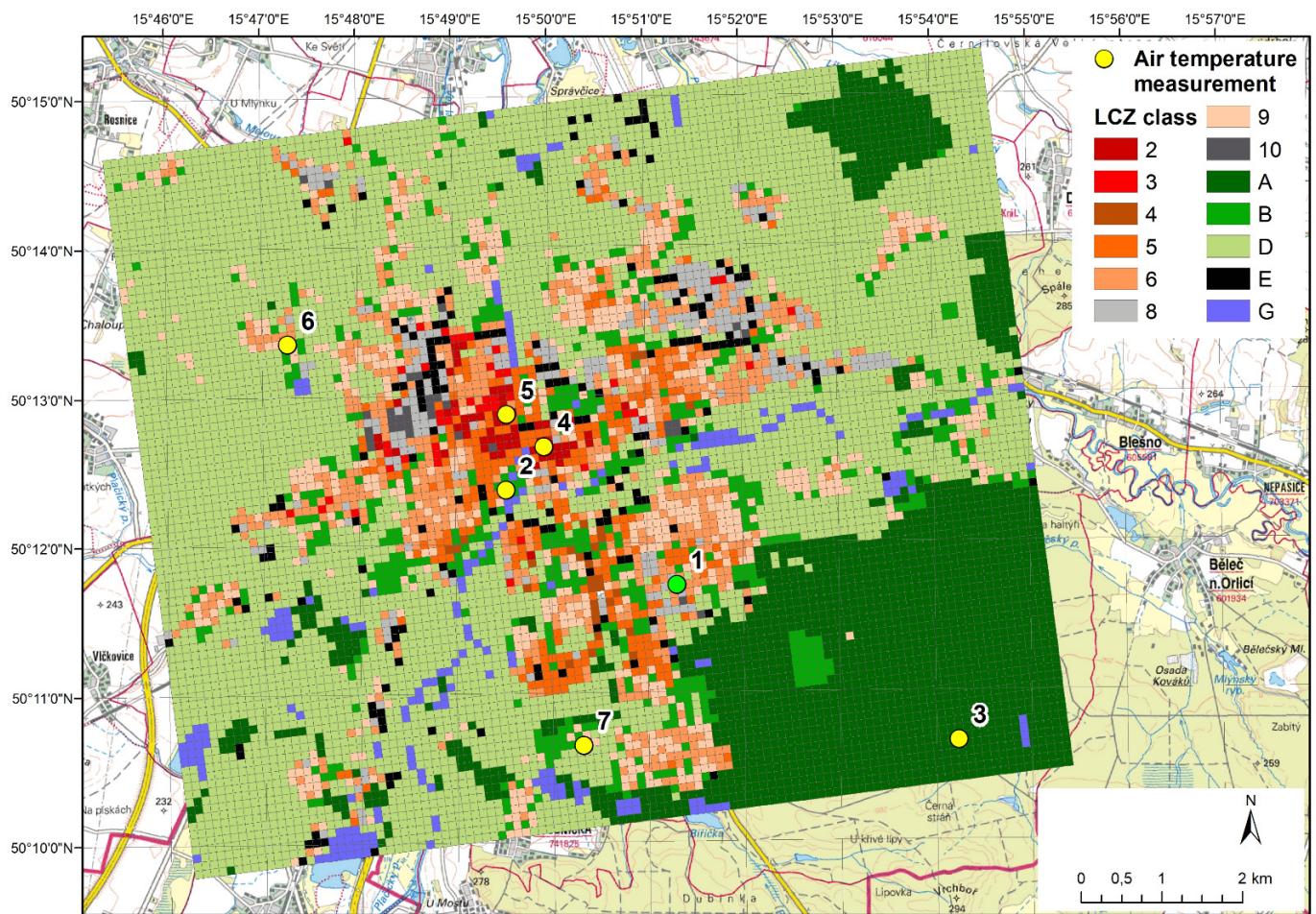


Figure 4. Delimiting local climate zones (LCZ) in Hradec Králové with marked AT measurement network—Section 2.3B (points numbered 1–7, when point number 1 indicates also location of field experiment described in Section 2.5). LCZ key: 2 compact mid-rise; 3 compact low-rise; 4 open high-rise; 5 open mid-rise; 6 open low-rise; 8 large low-rise; 9 sparsely built-up; 10 heavy industry; A dense trees; B scattered trees; D low plants; E bare rock or paved; G water. LCZs C and F do not either occur here or are represented only in a very limited amount, which does not allow objective analysis. Therefore, these were not included in the evaluation. Source: own processing based on classification algorithm [32].

Table 1. The total area of each LCZs in study area.

LCZ Class	2	3	4	5	6	8	9	10	A	B	D	E	G	SUM
Area (ha)	61	47	28	305	683	272	683	33	1838	577	4940	194	232	9893
Area (%)	0.6	0.5	0.3	3.1	6.9	2.7	6.9	0.3	18.6	5.8	49.9	2.0	2.3	100

Note: Remaining LCZ classes either are not represented in this case study or their area is negligible.

Table 2. Satellite imagery used for LST evaluation.

LANDSAT Scene Identifier	Date	Time (UTC)	Scene Cloud Cover	Solar Elevation	Solar Azimuth
LC81900252013169LGN01	2013/06/18	09:46:30	0.15	60.126	147.931
LC81910252013208LGN01	2013/07/27	09:52:42	1.65	55.684	148.656

The algorithm by [40] for the estimation of LST was used. LANDSAT-8 does not provide data for surface emissivity calculation. Because of this, a land surface emissivity algorithm was used, estimating emissivity from the normalized difference vegetation index (NDVI). Surface temperature data were processed using a mono-window algorithm, which considers a single frame in a thermal spectrum. The mono-window algorithm for

processing images from the LANDSAT-8 (TIRS sensor) satellite consists of two steps [41]. In this case, the brightness temperature represents the temperature of an absolutely black body at a given wavelength and radiation intensity. Within a selected range, however, the earth does not behave as an ideal emitter, and its emissivity is extremely variable over space. Therefore, a correction is necessary. The scheme of LANDSAT-8 scene processing is summarized in [33].

Statistical and graphical data processing employed software Origin 2018 (Origin-Lab Corporation, Northampton, MA, USA) and cluster analysis of plots using Ward's method [42] and Euclidean distance [43] in software STATISTICA 12 (StatSoft Czech Rep. s.r.o., the Czech Republic).

Area of interest (10×10 km) was divided into 10 000 cells (pixels) with 100×100 m, i.e., one-hectare area of each one. Being resampled to 30-m grid each cell then breaks down into 9 particular sub-cells.

For each relevant LCZ were then calculated following values:

"Average" value was derived as an average LST from all sub-cells falling into the LCZ in question.

"Abs min" is LST of the sub-cell with absolute minimum LST value in frame of the LCZ in question.

"Abs max" is LST of the sub-cell with absolute maximum LST value in frame of the LCZ in question.

"Mean min": the sub-cell with minimum LST was identified for each cell falling into the LCZ in question. LSTs of these sub-cells were subsequently averaged.

"Mean max": the sub-cell with maximum LST was identified for each cell falling into the particular LCZ. LSTs of these sub-cells were subsequently averaged.

This concept (evaluation based on both absolute and mean values of LST) has its logical and scientific reason, as seemingly homogenous LCZ may include significantly different microstructures. Relative representation of microstructure types in LCZ were published in [44] as case study on the city of Pilsen (Czech Republic, Central Europe). For instance, in frame of LCZ 8 they quantified also certain proportion of orchards and gardens, meadows and pastures, river and brook corridors, etc.

(B) Ad hoc monitoring of AT:

The network of AT and air humidity monitoring points (Table 3) was established in Hradec Králové and its surroundings in 2011 to analyze the influence of surface properties (land cover and land use) and its spatiotemporal variability. The sensors HOBO U23 Pro v2 Temperature/Relative Humidity (Onset Computer) placed inside a radiation shield 2 m above the ground, monitored the AT in various urban and suburban environments. Detailed description of measurement points can be found in previous studies [45,46]. The 10 min measurement step corresponds to the practice of the Czech Hydrometeorological Institute (CHMI), which operates a network of standard automatic climatic stations (AT sensors placed in a radiation shield two meters above the ground with grass cover) in order to monitor a macroclimate. Two CHMI climatic stations served as standard so as to determine temperature differences caused by specific land cover.

2.4. LST and AT Relation in LCZ

At the moment when the satellite was moving over the area of interest the instantaneous LST for a given LCZ was detected. All LSTs of all sub-cells from a given LCZ were averaged. The LCZs were then arranged accordingly from the highest to the lowest. In order to verify whether the warmest (coldest) LCZ in terms of LST also had the highest (lowest) AT, the instantaneous ATs were measured in the same minute in individual LCZs and then they were also arranged from highest to lowest.

Table 3. Location of the measurement and characteristics of the environment.

Location of Measurement	Label	Brief Characteristics of the Environment	LCZ [25] Classification in [46]	LCZ Class by [32]
Industrial zone 50°11'43.159'' N, 15°51'18.336'' E	1	significant proportion of horizontal concrete and asphalt surfaces, partial grassland, sunlit spaces all day	LCZ 8 _B (large low-rise with scattered trees)	8
City park 50°12'21.884'' N, 15°49'31.925'' E	2	woody vegetation in the city center, grass cover, full shade, near the confluence of two major rivers	LCZ B (scattered trees land cover type)	B
Suburban forest 50°10'39.974'' N, 15°54'14.036'' E	3	middle-aged, predominantly coniferous forest, shaded by trees (except in the afternoon), absence of significant artificial surfaces	LCZ A (dense trees land cover type)	A
Historic city center 50°12'39.493'' N, 15°49'55.767'' E	4	the historical part of the city center, enclosed area (courtyard) with vertical surfaces and limited air flow, artificial solid surfaces, insolation from morning until afternoon	LCZ 3 ₂ (compact low-rise with mid-rise built type)	2
Urban residential zone 50°12'52.516'' N, 15°49'32.781'' E	5	location surrounded by residential buildings five stories high, woody and shrubby vegetation in the immediate vicinity of the measurement location, grass cover, small summer swimming pool, partially sunlit afternoons	LCZ 2 _B (compact mid-rise with scattered trees)	2
Reference climatological location 50°13'21.367'' N, 15°47'15.969'' E	6	situated on the outskirts of suburban housing development, woody plants nearby, horizontal artificial surfaces nearby, located according to the principles of meteorological station establishment, the AT sensors are placed in a radiation shield	LCZ 9 (sparsely built–built type)	9
Reference climatological location 50°10'39.01'' N, 15°50'18.98'' E	7	situated on the outskirts of suburban housing development, woody plants nearby, significant areas of grass cover in the vicinity, located according to the principles of meteorological station establishment, the AT sensors are placed in a radiation shield	LCZ 9 (sparsely built–built type)	D

2.5. MUHI Evaluation: Measurement of Surface Temperature and Temperature of Adjacent Air

Artificial surfaces' temperature including the temperature of asphalt surface and temperature of adjacent air was monitored during carefully identified days, when particular attention was paid to the days with a high AT (tropical days) and a high value of global radiation, when the highest impact of artificial surfaces on AT is expected. Albedo effect on radiation reflection rate was specified by rough determination of the surface color shade on RAL CLASSIC scale, which represents a generally accepted standard in the building industry. The qualities of the surface materials in towns and cities, in terms of their emissivity (which determines the amount of long-wave radiation emitted by the surface, and as such the surface temperature), affect the surface temperature and consequently the air temperature.

Roof surface temperature was monitored in 10 min step by infrared thermometer Raytek MX2 with manual settings of emissivity. The sensor measures the amount of long wave radiation emitted from the monitored surface based on the Stefan–Boltzmann law and shows the surface temperature of the monitored subject. The amount of emitted radiation varies according to the physical and chemical properties of the surface. The recommended value for asphalt emissivity, $\epsilon = 0.93$, was used. The sensor measures the surface temperature with a resolution of 0.1 °C and an accuracy of 1.0 °C. AT at height of 5 cm, 50 cm, 100 cm a 200 cm above the monitored surface was measured in 10 min step by HOBO U23 Pro v2 Temperature/Relative Humidity (Onset Computer) sensors placed in radiation shields (the accuracy of the HOBO U23 V2 is 0.21 °C, with a resolution of 0.02 °C).

Global radiation in 10 min step was measured by CNR1 Kipp-Zonen (Delft, Netherland) sensor placed above monitored surface.

For more detailed observations of temperature stratification the measured data were interpolated by natural-neighbor method by Surfer software ver. 13 (Golden Software, Inc., Golden, CO, USA). Natural-neighbor interpolation is a fast, robust, and reliable technique for reconstructing a surface from irregularly distributed sample points. It faithfully preserves input data values and produces a continuous surface as its output. The technique is particularly useful for the kinds of unstructured data commonly encountered in geophysical applications.

3. Results

3.1. LST Evaluation

The results of the satellite thermal-image evaluation (18 June and 27 July 2013, approximately at 10 a.m. UTC) are presented in Table 4 and Figures 5–7. Figures 6C and 7C show up to 17 °C difference between minimum and maximum LST in the frame of a single one ha cell.

Table 4. LST (°C) in LCZ classes in study area.

		LCZ Class													
		2	3	4	5	6	8	9	10	A	B	D	E	G	AVG
18 June	Average	43.7	43.0	41.1	42.0	40.8	42.7	39.2	45.7	34.2	37.7	35.2	40.6	33.3	39.9
	Mean max	45.2	44.5	42.1	43.4	42.2	44.6	40.5	47.6	35.1	39.0	36.4	42.3	34.9	41.4
	Mean min	42.0	41.3	40.0	40.6	39.4	40.9	37.9	43.8	33.3	36.3	34.0	38.9	31.9	38.5
	Abs max	49.2	50.0	45.1	50.8	55.4	56.3	54.8	54.8	50.9	52.9	55.5	50.4	49.4	51.9
	Abs min	32.2	31.2	34.2	29.9	29.6	29.6	29.0	34.6	29.5	28.5	27.7	30.2	28.0	30.3
27 July	Average	45.7	45.6	45.3	45.1	44.0	45.6	42.8	47.8	36.0	41.6	40.3	44.0	37.1	43.1
	Mean max	47.0	46.9	46.0	46.4	45.3	47.4	44.1	49.5	37.0	43.0	41.6	45.5	38.9	44.5
	Mean min	44.2	44.2	44.5	43.8	42.8	43.9	41.6	46.3	35.0	40.3	39.0	42.6	35.4	41.8
	Abs max	51.2	51.0	49.4	54.9	57.6	57.7	55.6	57.1	53.3	54.5	57.9	54.0	56.3	54.7
	Abs min	38.1	37.0	40.4	34.1	33.4	34.7	32.8	37.9	31.9	32.6	31.0	34.8	30.5	34.6

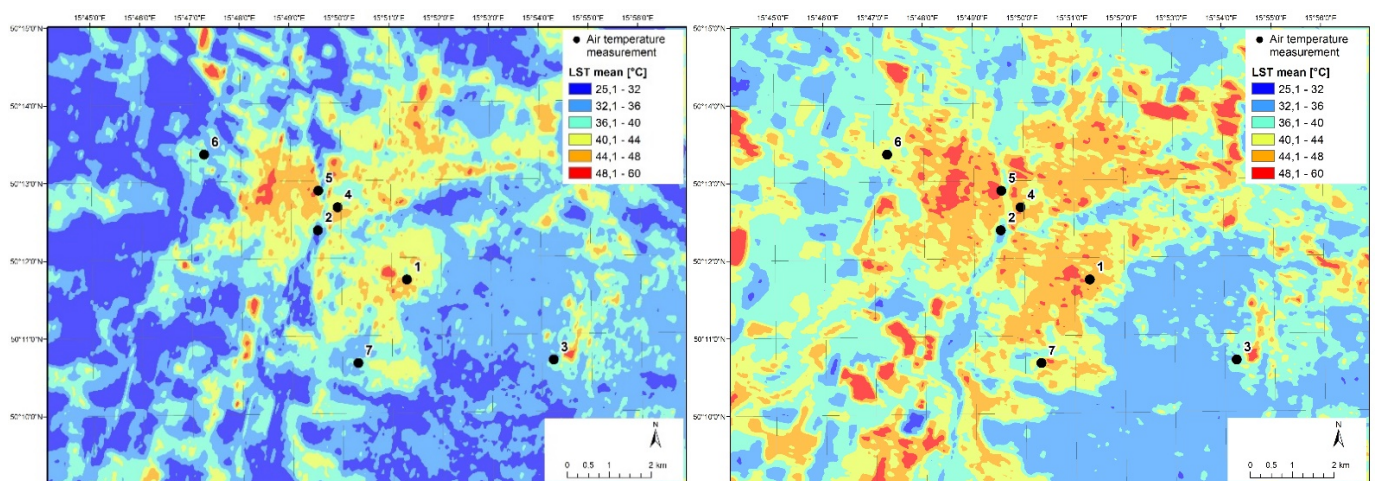


Figure 5. Land surface temperature in Hradec Králové and its surroundings, black dots (1–7) represent individual AT measurement sites; scene LC81900252013169LGN01 (left) and scene LC81910252013208LGN01 (right).

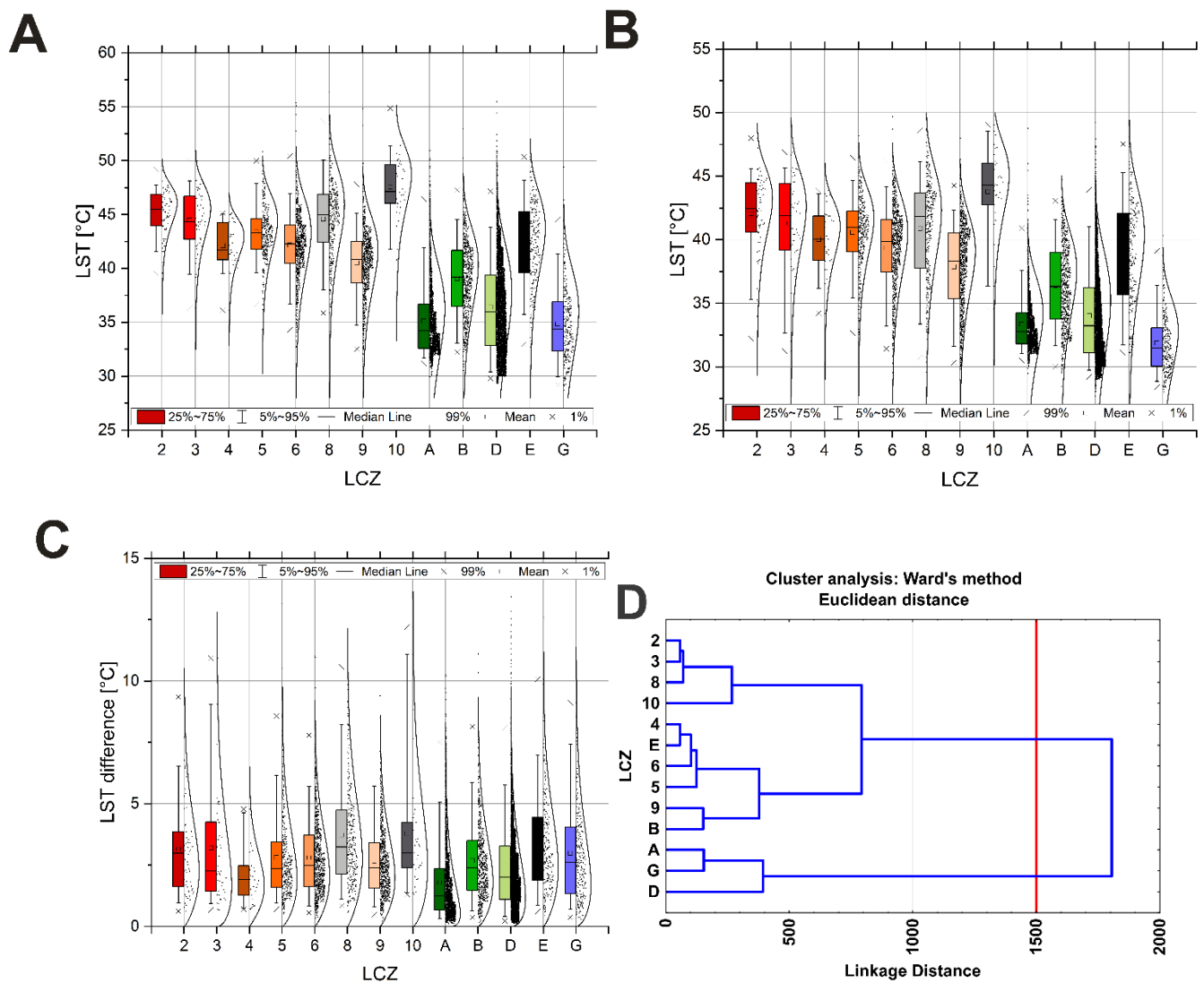


Figure 6. Box-plots with LSTs in LCZ classes in 18 June 2013; see Figure 3 for the LCZ key. Left up (A) mean maximum of LST; right up (B) mean minimum of LST; left down (C) mean difference (mean max LST minus mean min LST), values that are below /above the cross in the graph can be considered outliers when the cross symbolizes 1% of the values; right down (D) results of cluster analysis—the vertical red line represents the linkage chosen to select the clusters (red line in the cluster analysis refers to $\alpha = 0.05$ significance level).

LST in area of interest (Figure 5) varies mostly due to character of active surface, see Figure 3 (land use/land cover) and Figure 4 (spatial distribution of LCZs). Surface temperature markedly differs also with season (month), when great differences in surface temperature of vegetation are connected with growth stage and intensity of transpiration of individual species, stand density and its overall shape.

Heat accumulation in surfaces in culminating summer, reduced soil moisture affecting transpiration and terminal stage of vegetation caused the average LST of the July scene to be about 3.2 °C higher than that from June. Similar differences (ca 3 °C) respond also to both mean and absolute minimum and maximum LST. In addition, hot/cold spots in urban and sub-urban landscape were identified.

The highest June average LST and mean maximum LST correspond to LCZs 10, 2, 3 and 8 (Table 4; Figure 6A,B), i.e., land cover with distinct prevalence of artificial surfaces (heavy industry, compact mid-rise, compact low-rise, large low-rise). It testifies also a cluster of these LCZs on the dendrogram of cluster analysis on Figure 6D. Cluster analysis is the task of grouping a set of objects in such a way that objects in the same cluster are more

similar (in some sense) to each other than to those in other clusters. Analogously, another cluster is formed by LCZs A, G, D (dense trees, water, low plants) which significantly differs from all remaining LCZs in June.

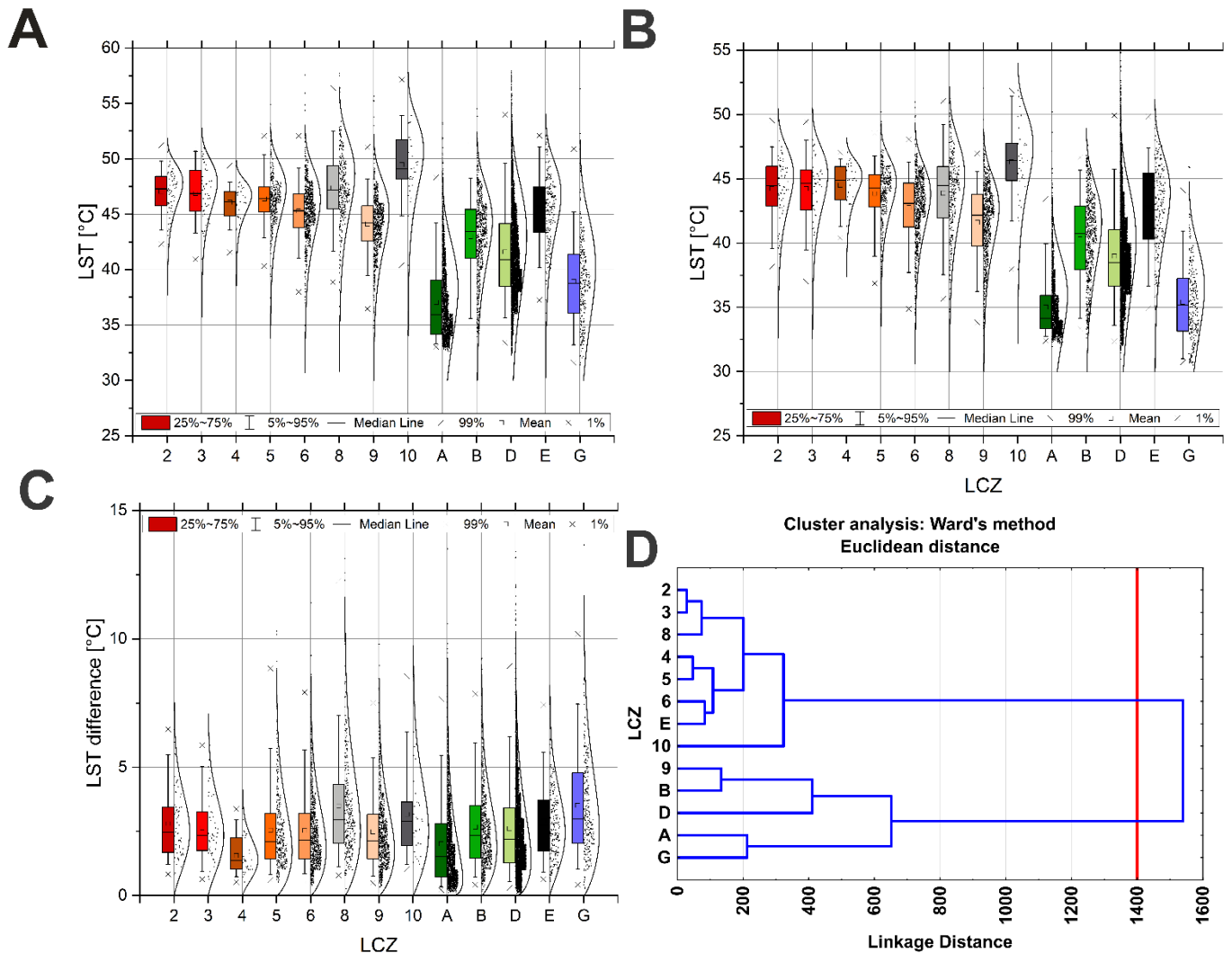


Figure 7. Box-plots with LSTs in LCZ classes in 27 July 2013; see Figure 3 for the LCZ key. Left up (A) mean maximum of LST; right up (B) mean minimum of LST; left down (C) mean difference (mean max LST minus mean min LST), values that are below/above the cross in the graph can be considered outliers when the cross symbolizes 1% of the values; right down (D) results of cluster analysis—the vertical red line represents the linkage chosen to select the clusters (red line in the cluster analysis refers to $\alpha = 0.05$ significance level).

In July, the values of average LST and mean maximum LST in most LCZs were close to each other (Table 4; Figure 7A,B). Significantly different from this unified cluster were only LSTs of LCZs 9, B, D, A and G—as demonstrated in the dendrogram of cluster analysis on Figure 7D. LST in these LCZs with abundant vegetation rate was significantly lower than in other LCZs (the second cluster). The highest average and mean max LST were reached in LCZ 10; nevertheless, the absolute maximum (57.7°C) was reached in LCZ 8.

A similar conclusion was reached in [20] in terms of the effect of radiant temperature on city dwellers for comparable Central European cities. During a heat wave, highly uncomfortable areas were identified as LCZ 2 (compact mid-rise), LCZ 3 (dense low-rise), LCZ 5 (open mid-rise), LCZ 8 (large low-rise) and LCZ 10 (heavy industry).

3.2. AT Evaluation

Study [46] published the result of AT monitoring for the area of interest, Hradec Králové (Table 5), and provided data for validation and verification of data delivered from remote sensing. In terms of average AT the LCZ 2 revealed as the hottest, followed by LCZ 8, LCZ D, LCZ B, LCZ 9 and LCZ A, which considerably corresponds also to the warm season (April to September), when the order of the zones was LCZ 2, LCZ 8, LCZ B, LCZ D, LCZ 9 and LCZ A.

Table 5. Basic statistical analysis of the AT over the entire period (August 2011–October 2014). Adapted from [46].

Location	LCZ Class by [32]	Avg	Median	Min	Max	Range	St. Dev.
1 (industrial zone)	8	11.0	10.8	−22.6	39.5	62.2	9.2
2 (city park)	B	10.6	11.0	−19.1	35.7	54.8	8.5
3 (suburban forest)	A	9.7	9.6	−22.5	37.3	59.7	8.8
4 (city center)	2	12.0	12.1	−17.7	41.1	58.8	9.3
5 (urban residential zone)	2	11.0	11.2	−18.6	36.2	54.8	8.7
6 (reference climatological location)	9	10.4	10.6	−20.1	36.8	56.9	8.8
7 (reference climatological location)	D	10.7	10.8	−18.4	37.2	55.6	8.7

The ATs at stations located in the compact rise (LCZ 2) were higher than in the open rise (LCZ 4, 5, and 6), sparsely built areas (LCZ 9) and on the outskirts of the city (LCZ B); the maximum daily temperatures were lowest in the compact rise (LCZ 2) and higher in the open rise (LCZ 4, 5, and 6) and on the outskirts of the city (LCZ B) in the experiment from similar conditions published by [47].

3.3. Interaction of LSTs Derived from Remote Sensing with Ground Monitoring of AT

The instantaneous LST and AT for a given LCZ were detected and arranged accordingly from the highest to the lowest (Table 6). However, the ATs were not measured in as many LCZs as LST. Therefore, in Table 6 is listed only those LCZs where both LST and ATs were measured. There is a logical assumption that when LST was the warmest in zone 2, it was expected to have also the highest AT, but it did not. It was the second highest. As a matter of fact, Table 6 shows what are/can be the relationships between LCZ, LST and AT.

Table 6. Confrontation of instantaneous LST and AT.

18 June	Average LST	43.7	42.7	39.2	37.7	35.2	34.2
	LCZ class	2	8	9	B	D	A
	AT	32.5	32.4	29.7	29.0	28.8	28.8
	LCZ class	8	2	9	D	B	A
27 July	Average LST	45.7	45.6	42.8	41.6	40.3	36.0
	LCZ class	2	8	9	B	D	A
	AT	35.9	35.8	32.5	32.3	31.0	30.9
	LCZ class	8	2	9	D	B	A

Even though the order of LCZs based on LST (from remote sensing) and their order based on AT do not fully correspond to each other, the correlation between LST and AT is statistically highly significant ($r = 0.929$, $p < 0.01$, $n = 6$) in June term and statistically significant in July term and for average value from both terms ($r = 0.853$ and $r = 0.895$ respectively, $p < 0.05$, $n = 6$). It proved a close dependence of AT on LST in respective LCZ. Similarly, the results in [48] show a connection between the land cover composition and air temperature by detecting an average temperature offset of about 1.5 °C between heavily urbanized and vegetated urban areas.

In contrast, [49] compared the surface temperature derived from thermal images with the AT from weather stations in vicinity of Olomouc city and found their relationship inconclusive.

3.4. MUHI Evaluation: Surface Temperature and Temperature of Adjacent Air

The data on surface temperature represent common artificial urban surface asphalt-shadow RAL 7043 (RGB 078-084-082)—traffic grey B. The data averaged from two representative days (both belonging to the heat wave, clear sky without cloudiness, windlessness, maximum AT in 2 m above grass at reference station above 30 °C) were graphically interpolated by Surfer software for more detailed presentation of temperature stratification (Figures 8 and 9). Figure 8 describes the vertical distribution of ATs above the artificial surface during the day with the AT higher than 30 °C. Not only the decrease of AT with increasing height above the surface (AT was monitored up to 200 cm), but also the temperature course during the warmest part of a tropical day is captured. This is important in terms of optimal term selection for taking satellite images for the LST evaluation within the UHI (SUHI) investigation.

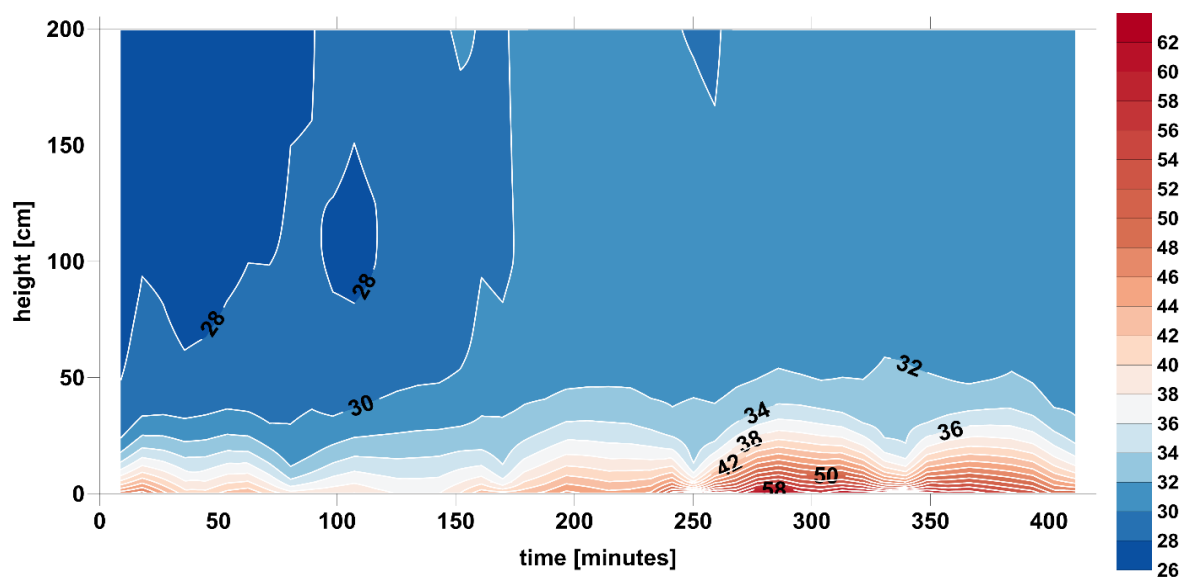


Figure 8. Temperature (°C) of common artificial urban surface asphalt and adjacent air during a cloudless tropical day. Axis x shows time from the point when the AT at 2 m at reference station reached 30 °C (approximately at 8 a.m. in this particular case).

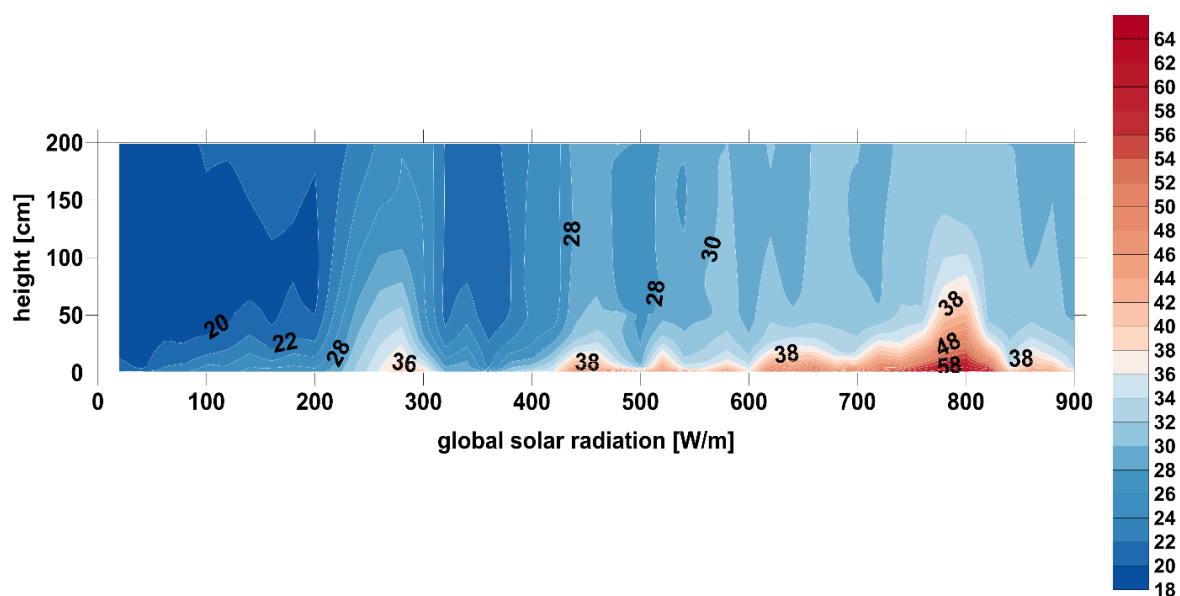


Figure 9. Temperature (°C) of common artificial urban surface asphalt and adjacent air during a cloudless tropical day—effect of global solar radiation (average from both representative days from sunrise to sunset).

Figure 9 describes the relationship of the AT above the artificial surface and the intensity of solar radiation (x -axis). The second independent variable in Figure 9 is the height above the surface (Y -axis). The dependence of AT on distance from the artificial surface and on the solar radiation during a tropical day is described. This is a significant result that should be taken into account, e.g., when dimensioning the location of urban vegetation, the location of the height of the technical infrastructure and, last but not least, placing the devices for monitoring the city's microclimate.

Daily course of temperature of investigated surface and adjacent air was fitted and defined by rational 2D function model. The obtained equation enables derivation of the AT at different heights from the surface temperature and vice versa, which is of great importance in terms of heat stress quantification (Figure 10).

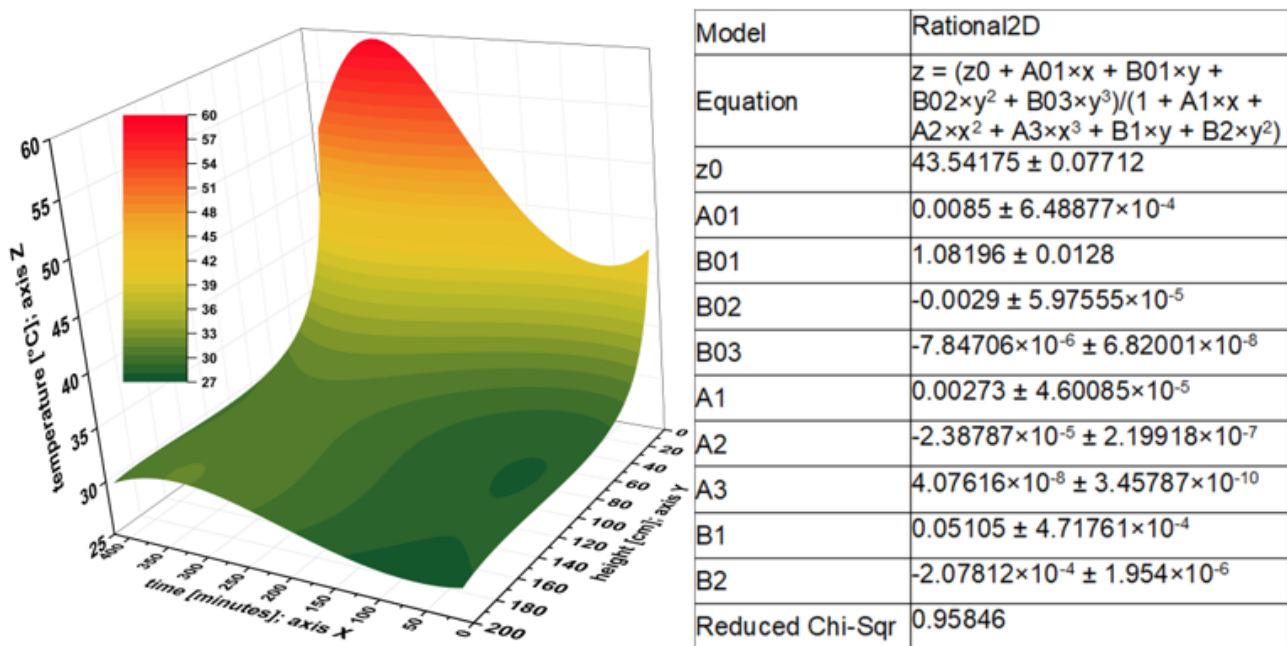


Figure 10. Fitted model of relationship between surface temperature (axis Z) and adjacent air mass temperature at different heights (axis Y “height”) and length of exposure to solar radiation during cloudless tropical day (axis X “time”) described by rational 2D function.

GIS-based derived LCZs and thermal remote sensing were combined together by adjusted model, forming a sophisticated tool, respecting the real character of the environment under investigation. It is obvious that the developed model is not universally (globally) valid, but it is contributory from methodological point of view.

4. Discussion

The near-surface AT measurements may seem to be best suited for analyzing temperature contrasts among LCZs [33], mainly in terms of evaluation of heat discomfort and its effect on human health. However, they are insufficient especially in terms of their ability to characterize temperature spatial distribution in detail, as their results depend on measurement network density, the used interpolation method, etc. Moreover, although over 60 heat stress indices have been proposed to assess high temperature environments and predict the possibility of heat strain for the body [50], they often neglect real UHI (MUHI) data. Their inputs mostly arise from macro-climatological observations, which significantly differ from UHI conditions. That is why the most appropriate method providing data for urban planning, creating and safeguarding healthy conditions appears to be models which would be able to derive AT from various airborne or satellite remote sensing systems as

a substitute for ground monitoring. The current real application of remote sensing often ends with the description of (inter)zonal temperature differences in surface of AT.

We confirmed a significant effect of the artificial surface on AT stratification in vertical profile. For example, during a continuous measurement of July 22–23 maximum temperature of surface and air at 5 and 200 cm above surface was 59.6, 35.3, and 31.9 °C, respectively. It corresponds well to solar radiation intensity and also to duration of surface heating (from sunrise) and sun angle. The results of [51] highlighted the key role of radiation in the spatiotemporal variability of thermal exposure in moderate-climate urban areas during summer days. Radiation directly affects thermal comfort through radiant temperature and indirectly through the complexity of turbulence in street canyons. The study of [52] also described the cooling effect of albedo in comparable zones in Central European cities (Brno and Praha) as daily average temperature dropped about 0.2 °C for albedo +0.25 and about 0.45 °C for albedo +0.50, while increasing the number of trees by 30% generally slightly lowers night-time temperature, and the cooling effect of additional trees on daily temperature does not exceed 0.2 °C.

All climatic categories are formed by active surface, but its effect is the most considerable on microclimate. The vegetation removing and unifying in areas with higher radiation balance increases temperature extremes and results in biological stress and discomfort. The results of [53] suggest a highly complex relationship between biometeorological indices and thermal sensation vote in urban environments, significantly influenced by specificity of place and time. Despite measured microclimatic effects that might indicate the opposite, the probability of thermal sensation vote-related heat stress is higher under trees and near sprayed water-mist. The differences in UTCI [50] (Universal Thermal Climate Index) values confirmed substantial cooling associated with high vegetation (trees induced differences up to 10.5 °C in UTCI), while the measurable cooling effect of low vegetation was negligible (not more than 2.3 °C UTCI) [54].

The impact of the UHI in Hradec Králové on city dwellers was evaluated by [36] using the HUMIDEX index. The highest HUMIDEX discomfort category incidence was in July followed by August. The city center (LCZ 2) was in this respect the most extreme location, followed by the LCZ 8 with concrete and asphalt surfaces. At places with artificial surfaces, discomfort categories begin in the morning and reached their maximum shortly after noon, while the great HUMIDEX discomfort in the hottest days (HUMIDEX above 40, where any exertion should be avoided) corresponds to afternoon (13.00 to 18.00 CEST), and some discomfort remained overnight.

The negative effects of UHI will probably be even stronger in the future, as [55,56] describe increasing annual number of days in heat waves from 6.13 days in 1961–1990 to 36 days in 2071–2100 for the central part of the Czech Republic. In addition, the climate change impact on plant phenology and thus reduction of induced cooling effect must also be taken into account. The vegetation period in 1990–2019 (209.2 days) was about 8 days longer than in 1961–1990 and its significant prolongation is also predicted by commonly respected climatic scenarios and models. A survey of [57] assumes that the ongoing warming of summer months will enhance evapotranspiration demands and will dry the environment. The negative effect of meteorological drought on the plant phenological phases will cause an earlier onset of leaf senescence and shortening of the growing season. It is worthy of highlighting here that the cooling effect of trees may range from 4 °C to 9 °C, and the cooling effect of grass in comparison with artificial paved surfaces in open public places may be from 2 °C to 5 °C UTCI [51].

The relationship between LST and AT at standard 2 m height is not always fully clear, especially in the case of massive share of green and blue infrastructure. Canopy microclimate in comparison with both macroclimate (standard climatological station) and urban climate (artificial urban surfaces), is characterized by lower temperature and humidity extremes, wetter environment, diffuse solar radiation and different air composition. Climatic differences between scattered trees (apple orchards) and climatological station were analyzed by [58], who documented an average up to 0.8 °C lower in air temperature

in scattered trees in growing season (April–October), while maximal short-term difference reached 5.9 °C. Physiologic processes of individual phenological phases are manifested by modification of moisture and temperature regime. Intensive transpiration of low vegetation thus might in the short-term show an even higher cooling effect than woods [59–61]. The increasing trend in the number and intensity of heat waves is likely to continue throughout the 21st century. Heat waves, often accompanied by drought, affect a wide variety of vegetation functions [62–65] and thus can implicate a negative effect on climatic functions of urban vegetation. This must be incorporated into frequently overoptimistic plans of vegetation placement in urban areas in order to mitigate the impact of climate change. In addition, re-designing a city on a large scale is typically illusionary, and planning measures are usually restricted to a small part of a city.

5. Conclusions

The case study to describe (inter)zonal surface temperature differences in Hradec Králové was performed based on remote sensing. In addition, hot/cold spots in urban and sub-urban landscape in terms of LST were identified. Subsequently, the (inter)zonal AT differences in Hradec Králové were compared with respective surface temperature differences. Based on surface temperature, we also attempted to derive the AT at different heights, which is of great importance in terms of heat stress quantification.

It is obvious that the developed model is not universally valid; however, it indicates the pathway for the construction of the complex approach which enables direct derivation of AT from remote sensing as a substitute for problematic ground monitoring. The complex approach could find an employment in a wide range of applications related to UHI negative impact on city dwellers.

We confirmed that in the case of LST LCZs 8, 10, 2 and 3 are the warmest, and in the case of AT we identified LCZs 8 and 2 as the warmest. Statistically significant correlation between LST and AT in the LCZs were identified. Nevertheless, there is no strict rule that the LCZ with the highest LST inevitably has also the highest AT. Even though there is a logical assumption that when LST is the warmest, the zone is expected to have also the highest AT, it does not. As a matter of fact, our results show what are/can be the relationships between LCZ, LST and AT. This is a significant result that should be taken into account when applying the concept of LST assessment in LCZs. Those LCZs are typical with high percentage of ISF (impervious surface fraction) where frequent material in Hradec Králové is asphalt on the ground (but also on the roofs). Therefore, it is particularly interesting to investigate how asphalt influences adjacent AT, which was performed here. This could help to understand/illustrate how much we could change (air) temperature in LCZ 8 and 10 when substantiating asphalt.

Author Contributions: Conceptualization, Hana Středová and Jaroslav Rožnovský; methodology, Tomáš Středa; software, Filip Chuchma; validation, Tomáš Středa and Filip Chuchma; formal analysis, Hana Středová; investigation, Jaroslav Rožnovský; resources, Tomáš Středa; writing—original draft preparation, Tomáš Středa; writing—review and editing, Hana Středová; visualization, Filip Chuchma; supervision, Jaroslav Rožnovský; project administration, Jaroslav Rožnovský; funding acquisition, Jaroslav Rožnovský. All authors have read and agreed to the published version of the manuscript.

Funding: This research was funded by the Internal Grant Agency of Faculty of Horticulture, Mendel University in Brno, grant No. IGA-ZF/2018-AP009.

Data Availability Statement: The data presented in this study are available on request from the corresponding author.

Conflicts of Interest: The authors declare no conflict of interest. The funders had no role in the design of the study; in the collection, analyses, or interpretation of data; in the writing of the manuscript, or in the decision to publish the results.

References

- Chuchma, F.; Středa, T.; Středová, H.; Rožnovský, J.; Vysoudil, M. Landscape Recreation and Bioclimatology—Hand in Hand. In Proceedings of the Conference on Public Recreation and Landscape Protection—with Nature Hand in Hand, Brno, Czech Republic, 2–4 May 2018; Fialová, J., Ed.; Mendel University in Brno: Brno, Czech Republic, 2018; pp. 232–237.
- Oke, T.R.; Johnson, G.T.; Steyn, D.G.; Watson, I.D. Simulation of surface urban heat islands under “ideal” conditions at night Part 2: Diagnosis of causation. *Bound-Lay. Meteorol.* **1991**, *56*, 339–358. [[CrossRef](#)]
- Matson, M.; McClain, E.P.; McGinnis, D.F., Jr.; Pritchard, J.A. Satellite detection of urban heat islands. *Mon. Weather Rev.* **1978**, *106*, 1725–1734. [[CrossRef](#)]
- Oke, T.R. The energetic basis of the urban heat island. *Q. J. Roy. Meteor. Soc.* **1982**, *108*, 1–24. [[CrossRef](#)]
- Howard, L. *The Climate of London Deduced from Meteorological Observations, Made in the Metropolis, and at Various Places Around it*; Harvey and Darton: London, UK, 1833; Volume 1–3.
- Tan, J.; Zheng, Y.; Song, G.; Kalkstein, L.S.; Kalkstein, A.J.; Tang, X. Heat wave impacts on mortality in Shanghai, 1998 and 2003. *Int. J. Biometeorol.* **2007**, *51*, 193–200. [[CrossRef](#)] [[PubMed](#)]
- Karl, T.; Knight, R. The 1995 Chicago heat wave: How likely is a recurrence? *B. Am. Meteorol. Soc.* **1997**, *78*, 1107–1120. [[CrossRef](#)]
- Dessai, S. Heat stress and mortality in Lisbon Part I. model construction and validation. *Int. J. Biometeorol.* **2002**, *47*, 6–12. [[CrossRef](#)]
- Schär, C.; Vidale, P.L.; Lüthi, D.; Frei, C.; Häberli, C.; Liniger, M.A.; Appenzeller, C. The role of increasing temperature variability in European summer heatwaves. *Nature* **2004**, *427*, 332–336. [[CrossRef](#)]
- Smargiassi, A.; Goldberg, M.S.; Plante, C.; Fournier, M.; Baudouin, Y.; Kosatsky, T. Variation of daily warm season mortality as a function of micro-urban heat islands. *J. Epidemiol. Commun. Health* **2009**, *63*, 659–664. [[CrossRef](#)]
- Arsenović, D.; Lehnert, M.; Fiedor, D.; Šimáček, P.; Středová, H.; Středa, T.; Savić, S. Heat-waves and mortality in Czech cities: A case study for the summers of 2015 and 2016. *Geographica Pannonica* **2019**, *23*, 162–172. [[CrossRef](#)]
- Meehl, G.A.; Tebaldi, C. More intense, More frequent, and longer lasting heat waves in the 21st century. *Science* **2004**, *305*, 994–997. [[CrossRef](#)]
- Zubidat, A.E.; Haim, A. Artificial light-at-night-a novel lifestyle risk factor for metabolic disorder and cancer morbidity. *J. Basic Clin. Physiol. Pharmacol.* **2017**, *28*, 295–313. [[CrossRef](#)]
- Kanianska, R.; Škvareninová, J.; Kaniansky, S. Landscape potential and light pollution as key factors for astrotourism development: A case study of a Slovak Upland region. *Land* **2020**, *9*, 374. [[CrossRef](#)]
- Škvareninová, J.; Tuhárska, M.; Škvarenina, J.; Babálová, D.; Slobodníková, L.; Slobodník, B.; Středová, H.; Mind’áš, J. Effects of light pollution on tree phenology in the urban environment. *Morav. Geogr. Rep.* **2017**, *25*, 282–290. [[CrossRef](#)]
- Błażejczyk, K.; Epstein, Y.; Jendritzky, G.; Staiger, H.; Tinz, B. Comparison of UTCI to selected thermal indices. *Int. J. Biometeorol.* **2012**, *56*, 515–535. [[CrossRef](#)]
- Aniello, C.; Morgan, K.; Busbey, A.; Newland, L. Mapping micro-urban heat islands using LANDSAT TM and a GIS. *Comput. Geosci.* **1995**, *21*, 965–969. [[CrossRef](#)]
- Ekşi, M.; Uzun, A. Investigation of thermal benefits of an extensive green roof in Istanbul climate. *Sci. Res. Essays* **2013**, *8*, 623–632. [[CrossRef](#)]
- Stathopoulou, M.; Cartalis, C.; Keramitsoglou, I. Mapping micro-urban heat islands using NOAA/AVHRR images and CORINE Land Cover: An application to coastal cities of Greece. *Int. J. Remote Sens.* **2004**, *25*, 2301–2316. [[CrossRef](#)]
- Peng, S.; Piao, S.; Ciais, P.; Friedlingstein, P.; Ottle, C.; Bréon, F.M.; Nan, H.; Zhou, L.; Myneni, R.B. Surface urban heat island across 419 global big cities. *Environ. Sci. Technol.* **2012**, *46*, 696–703. [[CrossRef](#)]
- Geletiĉ, J.; Lehnert, M.; Savić, S.; Milošević, D. Inter-/intra-zonal seasonal variability of the surface urban heat island based on local climate zones in three central European cities. *Build. Environ.* **2019**, *156*, 21–32. [[CrossRef](#)]
- Vysoudil, M.; Létal, A.; Pavelková, R. Thermal monitoring: Identification tool of natural disasters risks response to local climatic effects. In Proceedings of the 33rd International Symposium on Remote Sensing of Environment, ISRSE 2009, Stresa, Italy, 4–8 May 2009; code 97459. pp. 571–574.
- Ellefsen, R. Mapping and measuring buildings in the canopy boundary layer in ten U.S. cities. *Energy Build.* **1991**, *16*, 1025–1049. [[CrossRef](#)]
- Oke, T.R. Initial Guidance to Obtain Representative Meteorological Observations at Urban Sites. IOM Rep. 81, 2004, WMO/TD-No. 1250, 47p. Available online: www.wmo.int/pages/prog/www/IMOP/publications/IOM-81/IOM-81-UrbanMetObs.pdf (accessed on 4 March 2021).
- Stewart, I.D.; Oke, T.R. Local climate zones for urban temperature studies. *B. Am. Meteorol. Soc.* **2012**, *93*, 1879–1900. [[CrossRef](#)]
- Bechtel, B.; Daneke, C. Classification of local climate zones based on multiple earth observation data. *IEEE J. Sel. Top. Appl.* **2012**, *5*, 1191–1202. [[CrossRef](#)]
- Lelovics, E.; Unger, J.; Gál, T.; Gál, C.V. Design of an urban monitoring network based on Local Climate Zone mapping and temperature pattern modelling. *Clim. Res.* **2014**, *60*, 51–62. [[CrossRef](#)]
- Lehnert, M.; Savić, S.; Milošević, D.; Dunjić, J.; Geletiĉ, J. Mapping local climate zones and their applications in European urban environments: A systematic literature review and future development trends. *ISPRS Int. J. Geo-Inf.* **2021**, *10*, 260. [[CrossRef](#)]
- Bechtel, B.; Alexander, P.J.; Böhner, J.; Ching, J.; Conrad, O.; Feddema, J.; Mills, G.; See, L.; Stewart, I. Mapping Local Climate Zones for a Worldwide Database of the Form and Function of Cities. *ISPRS Int. J. Geo-Inf.* **2015**, *4*, 199–219. [[CrossRef](#)]

30. Bokwa, A.; Hajto, M.J.; Walawender, J.P.; Szymanowski, M. Influence of diversified relief on the urban heat island in the city of Kraków, Poland. *Theor. Appl. Climatol.* **2015**, *122*, 365–382. [CrossRef]
31. Leconte, F.; Bouyer, J.; Claverie, R.; Pétrissans, M. Using local climate zone scheme for UHI assessment: Evaluation of the method using mobile measurements. *Build. Environ.* **2015**, *83*, 39–49. [CrossRef]
32. Geletič, J.; Lehnert, M. GIS-based delineation of local climate zones: The case of medium-sized Central European cities. *Morav. Geogr. Rep.* **2016**, *24*, 2–12. [CrossRef]
33. Geletič, J.; Lehnert, M.; Dobrovolný, P. Land surface temperature differences within local climate zones, based on two Central European cities. *Remote Sens.* **2016**, *8*, 788. [CrossRef]
34. Yan, H.; Yang, S.; Guo, X.; Wu, F.; Wu, R.; Shao, F.; Bao, Z. Impact of land cover composition and structure on air temperature based on the local climate zone scheme in Hangzhou, China. *Atmosphere* **2021**, *12*, 936. [CrossRef]
35. Cai, M.; Ren, C.; Xu, Y.; Lau, K.K.-L.; Wang, R. Investigating the relationship between local climate zone and land surface temperature using an improved WUDAPT methodology—A case study of Yangtze River delta, China. *Urban Clim.* **2018**, *24*, 485–502. [CrossRef]
36. Rožnovský, J.; Litschmann, T.; Středová, H.; Středa, T.; Salaš, P.; Horká, M. Microclimate evaluation of the Hradec Králové city using HUMIDEX. *Contrib. Geophys. Geod.* **2017**, *47*, 231–246. [CrossRef]
37. Köppen, W. Die Wärmezonen der Erde, nach der Dauer der heißen, gemässigten und kalten Zeit und nach der Wirkung der Wärme auf die organische Welt betrachtet. *Meteorol. Z.* **1884**, *1*, 215–226.
38. European Environment Agency (EEA). Copernicus Programme. Urban Atlas 2018. Available online: <https://land.copernicus.eu/local/urban-atlas> (accessed on 5 April 2021).
39. U.S. Geological Survey. EarthExplorer. Available online: <https://earthexplorer.usgs.gov> (accessed on 5 April 2021).
40. Rozenstein, O.; Qin, Z.; Derimian, Y.; Karnieli, A. Derivation of land surface temperature for Landsat-8 TIRS using a split window algorithm. *Sensors* **2014**, *14*, 5768–5780. [CrossRef]
41. Weng, Q. Thermal infrared remote sensing for urban climate and environmental studies: Methods, applications, and trends. *ISPRS J. Photogramm.* **2009**, *64*, 335–344. [CrossRef]
42. Ward, J.H. Hierarchical grouping to optimize an objective function. *J. Am. Stat. Assoc.* **1963**, *58*, 236–244. [CrossRef]
43. Murtagh, F.; Legendre, P. Ward’s hierarchical agglomerative clustering method: Which algorithms implement Ward’s criterion? *J. Classif.* **2014**, *31*, 274–295. [CrossRef]
44. Kopp, J.; Frajer, J.; Novotná, M.; Preis, J.; Dolejš, M. Comparison of Ecohydrological and Climatological Zoning of the Cities: Case Study of the City of Pilsen. *ISPRS Int. J. Geo-Inf.* **2021**, *10*, 350. [CrossRef]
45. Středa, T.; Středová, H.; Šedivá, I. Bioclimatic conditions for the recreationally important areas in the medium size city. In *Public Recreation and Landscape Protection—with Man Hand in Hand? Krtiny, Czech Republic, 5–6 May 2014*; Mendel University in Brno: Brno, Czech Republic, 2014; pp. 47–51.
46. Středová, H.; Středa, T.; Litschmann, T. Smart tools of urban climate evaluation for smart spatial planning. *Morav. Geogr. Rep.* **2015**, *23*, 47–57. [CrossRef]
47. Lehnert, M.; Geletič, J.; Husák, J.; Vysoudil, M. Urban field classification by “local climate zones” in a medium-sized Central European city: The case of Olomouc (Czech Republic). *Theor. Appl. Climatol.* **2015**, *122*, 531–541. [CrossRef]
48. Oxoli, D.; Ronchetti, G.; Minghini, M.; Molinari, M.E.; Lotfian, M.; Sona, G.; Brovelli, M.A. Measuring urban land cover influence on air temperature through multiple geo-data—The case of Milan, Italy. *ISPRS Int. J. Geo-Inf.* **2018**, *7*, 421. [CrossRef]
49. Geletič, J.; Vysoudil, M. Analysis of surface temperatures in urban and suburban landscapes from satellite thermal images: A case study of Olomouc and its environs, Czech Republic. *Morav. Geogr. Rep.* **2012**, *20*, 2–15.
50. Zare, S.; Hasheminejad, N.; Shirvan, H.E.; Hemmatjo, R.; Sarebanzadeh, K.; Ahmadi, S. Comparing Universal Thermal Climate Index (UTCI) with selected thermal indices/environmental parameters during 12 months of the year. *Weather. Clim. Extrem.* **2018**, *19*, 49–57. [CrossRef]
51. Geletič, J.; Lehnert, M.; Krč, P.; Resler, J.; Krayenhoff, E.S. High-resolution modelling of thermal exposure during a hot spell: A case study using PALM-4U in Prague, Czech Republic. *Atmosphere* **2021**, *12*, 175. [CrossRef]
52. Geletič, J.; Lehnert, M.; Jurek, M. Spatiotemporal variability of air temperature during a heat wave in real and modified landcover conditions: Prague and Brno (Czech Republic). *Urban Clim.* **2020**, *31*, 100588. [CrossRef]
53. Lehnert, M.; Brabec, M.; Jurek, M.; Tokar, V.; Geletič, J. The role of blue and green infrastructure in thermal sensation in public urban areas: A case study of summer days in four Czech cities. *Sustain. Cities Soc.* **2021**, *66*, 102683. [CrossRef]
54. Lehnert, M.; Tokar, V.; Jurek, M.; Geletič, J. Summer thermal comfort in Czech cities: Measured effects of blue and green features in city centres. *Int. J. Biometeorol.* **2021**, *65*, 1277–1289. [CrossRef]
55. Vaníčková, M.; Stehnová, E.; Středová, H. Long-term development and prediction of climate extremity and heat waves occurrence: Case study for agricultural land. *Contrib. Geophys. Geod.* **2017**, *47*, 247–260. [CrossRef]
56. Středová, H.; Středa, T. Agroclimatic conditions of the Czech Republic—Development and influence on agricultural production. In *Seed and Seedlings, Prague, Czech Republic*; Pazderu, K., Ed.; Czech University of Life Sciences: Prague, Czech Republic, 2015; pp. 22–27.
57. Lukášová, V.; Vido, J.; Škvareninová, J.; Bičárová, S.; Hlavatá, H.; Borsányi, P.; Škvarenina, J. Autumn phenological response of European beech to summer drought and heat. *Water* **2020**, *12*, 2610. [CrossRef]

58. Středa, T.; Středová, H.; Rožnovský, J. Orchards microclimatic specifics. In *Bioclimate: Source and Limit of Social Development, Topolčianky, Slovakia*; Slovak University of Agriculture: Nitra, Slovakia, 2011; pp. 132–133.
59. Středa, T.; Cerkal, R.; Hájková, L.; Chuchma, F.; Khel, T.; Klimešová, J. GIS application in abiotic risks regionalization for spring barley. *Contrib. Geophys. Geod.* **2020**, *50*, 49–60. [[CrossRef](#)]
60. Litschmann, T.; Středa, T. Surface temperature of plant tissues. Which method of air temperature measurement fits best? *Contrib. Geophys. Geod.* **2019**, *49*, 11–23. [[CrossRef](#)]
61. Středa, T.; Středová, H.; Chuchma, F.; Kučera, J.; Rožnovský, J. Smart method of agricultural drought regionalization: A winter wheat case study. *Contrib. Geophys. Geod.* **2019**, *49*, 25–36. [[CrossRef](#)]
62. Středová, H.; Fukalová, P.; Chuchma, F.; Středa, T. A complex method for estimation of multiple abiotic hazards in forest ecosystems. *Water* **2020**, *12*, 2872. [[CrossRef](#)]
63. Středová, H.; Klimešová, J.; Středa, T.; Fukalová, P. Could the directly measured data of transpiration be replaced by model outputs? *Contrib. Geophys. Geod.* **2020**, *50*, 33–47. [[CrossRef](#)]
64. Babálová, D.; Škvareninová, J.; Fazekaš, J.; Vyskot, I. The dynamics of the phenological development of four woody species in South-West and Central Slovakia. *Sustainability* **2018**, *10*, 1497. [[CrossRef](#)]
65. Středa, T.; Středová, H.; Rožnovský, J. Microclimate of tourist attractive areas of Brno City. In *Public Recreation and Landscape Protection—Hand in Hand? Brno, Czech Republic, 4–6 May 2011*; Fialová, J., Ed.; Mendel University in Brno: Brno, Czech Republic, 2011; pp. 78–84.